Article

SOURCE DATA | TRANSPARENT PROCESS | OPEN ACCESS

EMBO reports

Cyclic expression of the voltage-gated potassium channel K_V10.1 promotes disassembly of the primary cilium

Araceli Sánchez, Diana Urrego & Luis A Pardo*

Abstract

The primary cilium, critical for morphogenic and growth factor signaling, is assembled upon cell cycle exit, but the links between ciliogenesis and cell cycle progression are unclear. K_V10.1 is a voltage-gated potassium channel frequently overexpressed in tumors. We have previously reported that expression of K_V10.1 is temporally restricted to a time period immediately prior to mitosis in healthy cells. Here, we provide microscopical and biochemical evidence that K_V10.1 localizes to the centrosome and the primary cilium and promotes ciliary disassembly. Interference with K_V10.1 ciliary localization abolishes not only the effects on ciliary disassembly, but also K_V10.1-induced tumor progression *in vivo*. Conversely, upon knockdown of K_V10.1, ciliary disassembly is impaired, proliferation is delayed, and proliferating cells show prominent primary cilia. Thus, modulation of ciliogenesis by K_V10.1 can explain the influence of K_V10.1 expression on the proliferation of normal cells and is likely to be a major mechanism underlying its tumorigenic effects.

Keywords cell cycle; K_V10.1; primary cilium
Subject Categories Cell Cycle; Membrane & Intracellular Transport
DOI 10.15252/embr.201541082 | Received 26 July 2015 | Revised 3 March 2016 | Accepted 9 March 2016 | Published online 21 April 2016
EMBO Reports (2016) 17: 708–723

Introduction

Cellular functions of voltage-gated potassium channels include the regulation of the resting membrane potential in both excitable and non-excitable cells, modulation of cellular volume, and proliferation [1]. K_V10.1 (*KCNH1*, Eag1) is a voltage-gated potassium channel widely expressed in the human brain, but practically undetectable in peripheral tissues. Interestingly, K_V10.1 is frequently up-regulated in human cancers, where its expression contributes to tumor progression and correlates with poorer prognosis in several tumor types [2]. Tumor cells expressing K_V10.1 appear to acquire selective advantages such as resistance to hypoxic environments [3] that allow them to sustain chronic proliferation. The exact mechanism responsible both for K_V10.1 aberrant expression and its impact on the pathophysiology of cancer cells is not well understood.

In tissues, quiescent cells assemble a primary cilium. This is an antenna-like microtubule-based structure that senses chemical or physical stimuli from the extracellular milieu [4]. Signaling activity at the primary cilium can regulate cell proliferation, and its assembly/disassembly might also influence cell cycle entry. In postmitotic cells in G0/G1, the mother centriole differentiates into the basal body, attaches to the plasma membrane, and nucleates the primary cilium [5]. During mitosis, release of the mother centriole from the cilium is a prerequisite for the centrosome to play its role as microtubule-organizing center for the spindle. Therefore, resorption or disassembly of primary cilium is thought to be required prior to mitosis (reviewed, e.g., in [6]). Improper formation or absence of primary cilia impair the cellular responses to differentiation signals, leading to a group of diseases collectively termed ciliopathies, that show common clinical features, such as visceral cysts, defective digits, oral anomalies, cognitive impairment, and tumors (e.g., [7–11]).

The exact mechanism that coordinates the timing of cilia assembly/disassembly with the cell cycle is still unclear. Cell cycle regulators (e.g., APC, cyclin B1, and Aurora A [12–14]), Rab GTPases contributing to vesicle transport [15,16], and proteins implicated in actin cytoskeleton architecture and dynamics [17] are all important for ciliary disassembly prior to mitosis [18–20].

We have previously shown that K_V10.1 interacts with proteins that participate in ciliary regulation, such as Rabaptin 5 (RabEP1) [21], cortactin (CTT) [22], and HIF (through VHL) [3], and we and others have observed that K_V10.1 transcription is transiently activated in response to E2F1 activity in cells undergoing cell division [1,18]. K_V10.1 expression occurs therefore when the primary cilium must be disassembled for cells to divide. We show here that expression of K_V10.1 induces ciliary disassembly. Conversely, inhibition of K_V10.1 expression causes aberrant ciliogenesis in actively proliferating cells. These results account for the sustained growth observed in cells aberrantly expressing K_V10.1 [23]. They also explain the fact that gain-of-function mutations in K_V10.1 lead to developmental alterations akin to ciliopathies (Temple–Baraitser and Zimmermann–Laband syndromes among others) [24–26].

Oncophysiology Group, Max-Planck-Institute of Experimental Medicine, Göttingen, Germany
*Corresponding author. Tel: +49 551 3899 643; E-mail: pardo@em.mpg.de

Results

K_V10.1 overexpression reduces the occurrence of primary cilia

Actively proliferating cells do not normally bear a primary cilium [27], because cilium resorption starts as soon as cells reenter the cell cycle [14]. While studying the influence of K_V10.1 in cell cycle progression, we intended to use the presence of a primary cilium as indication of quiescence. We then noticed that in serum-starved cultures of NIH3T3 cells transfected with K_V10.1 fused to EGFP, those cells overexpressing K_V10.1-EGFP (fixed and stained with anti-acetylated α-tubulin), were always devoid of cilia (Fig 1A). To achieve a quantitative measurement of this phenomenon, we studied the frequency of ciliation in cultured NIH3T3 mouse fibroblasts actively proliferating in the presence of FCS, which amounted to 37.4 ± 23% (N = 35; acetylated α-tubulin immunostaining; Fig 1B). Serum withdrawal for 24 h arrested the cell cycle and thereby doubled the fraction of ciliated cells (67.3 ± 22.7%, N = 37; Fig 1B). As expected, subsequent reintroduction of serum (for 4 h) to induce reinitiation of the cell cycle decreased again the fraction of ciliated cells (to 46.6 ± 23%, N = 36). In cells transfected with K_V10.1 under the control of a strong promoter (CMV), the fraction of ciliated cells decreased under all tested conditions (Fig 1B, red bars).

The effect was not cell-type specific; similar results were obtained in hTERT-RPE1 (immortalized retinal pigmented epithelial cells [28]) upon overexpression of K_V10.1 (Fig 1C). Transfection of another potassium channel, K_V10.2, which is very similar to K_V10.1 from a functional point of view and shares 73% homology at the primary sequence [29–31], did not induce a reduction in the abundance of ciliated cells (inset in Fig 1C), indicating that not all potassium channels share this property. Finally, the same result was observed using any of the cilium markers anti-acetylated α-tubulin (Fig 1C), anti-Arl13B (Fig 1D), or anti-detyrosinated tubulin, indicating that it is a genuine change in the abundance of cilia.

K_V10.1 knockdown induces aberrant ciliogenesis in proliferating cells

hTERT-RPE1 cells express significant endogenous levels of K_V10.1 (Fig EV1). In exponentially growing cultures, the low frequency of ciliated cells in complete medium was not significantly decreased by overexpression of K_V10.1 (Fig 2B). However, in cells starved for 24 h, partial knockdown of K_V10.1 (Fig EV1) induced ciliogenesis in a large fraction of cells (Fig 2A–C) and increased the length of the cilia therein (5.12 ± 3.21 vs. 4.18 ± 2.51 μm, $P < 0.001$, two-way ANOVA, see Fig 2D). Upon reintroduction of serum, the control cells immediately started ciliary disassembly and the number and length of cilia decreased rapidly (Fig 2C and D). Both the number and length of cilia increased again after 5 h, which could obey to a second wave of re-ciliation in late G1/S as described in [12,32]. We observed increased frequency of ciliated cells at all times tested, as well as in the continuous presence of serum; we therefore cannot exclude the implication of K_V10.1 in either of the two waves of ciliation. K_V10.1-knockdown cells maintained both the abundance and the length of their cilia for significantly longer periods than untreated cells, indicating that the presence of K_V10.1 accelerates ciliary disassembly. This conclusion was reinforced by the observation that pharmacological blockade of K_V10.1 using astemizole (10 μM; [33]) also delayed deciliation (Fig 2E). Furthermore, typically non-ciliated cells like HeLa [34] (but see also [35]), whose cell cycle is slowed down by K_V10.1 knockdown [1], showed cilia upon transfection with K_V10.1 siRNA (Fig EV2).

The effects observed upon overexpression of K_V10.1 (Fig 1) are not exactly opposite to those described in Fig 2, but rather a combination of acceleration of disassembly and inhibition of reciliation. The latter effect is mechanistically different (e.g., it does not depend on permeation of potassium, Fig EV3). For the sake of clarity, we will focus our discussion on ciliary resorption from now on and refer the reader to the Expanded View information in Fig EV3 for further details.

Consistently with the experiments in Fig 2, when we tested the presence of cilia in primary mouse embryonic fibroblasts (MEFs), we also observed a clear increase in the number of ciliated cells in MEFs from K_V10.1 knockout mice [36] in comparison with wild-type controls (Fig 3A; data from ten embryos each from two litters). Transfection of human K_V10.1 rescued the phenotype, and the number of cilia decreased strongly (Fig 3B); in cells co-transfected with K_V10.1 and mVenus, the presence of Venus fluorescence (indicating successfully transfected cells) and primary cilia were mutually exclusive (Fig 3C) indicating that the increase in ciliated cells in knockout MEFs is directly attributable to the absence of K_V10.1.

Gain-of-function mutations of the gene encoding for K_V10.1 (*KCNH1*) cause Temple–Baraitser and Zimmermann–Laband syndromes [24,25]. Both diseases show orofacial and digital abnormalities (together with severe mental retardation), and their morphological features are highly reminiscent of ciliopathies. We generated a mutant K_V10.1 (L352V) described in Zimmermann–Laband patients. The ion channel is activated at much more negative potential than the wild type (Fig EV4) and is therefore active at rest. We transfected the mutant channel into wild-type MEFs and tested its effect on ciliary resorption (as above, by serum starvation and subsequent reintroduction of serum for 4 h). Wild-type K_V10.1 dramatically reduced the percentage of cells showing cilia, and as predicted, the mutant further reduced the amount of ciliated cells (Fig 3D).

Among the signaling pathways where integrity of the primary cilium is important, sonic hedgehog (SHH) [37] is a relevant factor for a variety of cancers [38]. It is well established that SHH signaling is spatially confined to the primary cilium. In the absence of the SHH ligand, the downstream Gli transcription factors are processed at the primary cilium to render their repressor forms. Therefore, an increased number of cilia reinforce activation by SHH (e.g., [39]). To test the activity and integrity of the SHH pathway, we determined the abundance of mRNA for *Gli1*, which reflects activation of the pathway. Cells were serum-starved for 48 h in the presence or absence of recombinant human SHH; cells obtained from knockout mice showed much higher sensitivity to SHH pathway activation (Fig 3E). Using a RT–PCR array for the SHH pathway, MEFs from knockout mice under serum starvation showed a significant increase of basal levels (compared to wild-type MEFs) of a number of genes implicated in SHH signaling (such as *Gas1, Smo, Gli2, Sufu, Zic2, Disp2, and Shox2*) and in pathways that cross talk with SHH: TGFβ/BMP (*Bmp7*), Wnt (*Wnt2, 2b, 4, 5b, and 6, Wif1*), and Hippo (*Stk3*) (Fig EV5). Addition of SHH for 48 h induced an increase in the levels of markers for SHH activation, in many cases

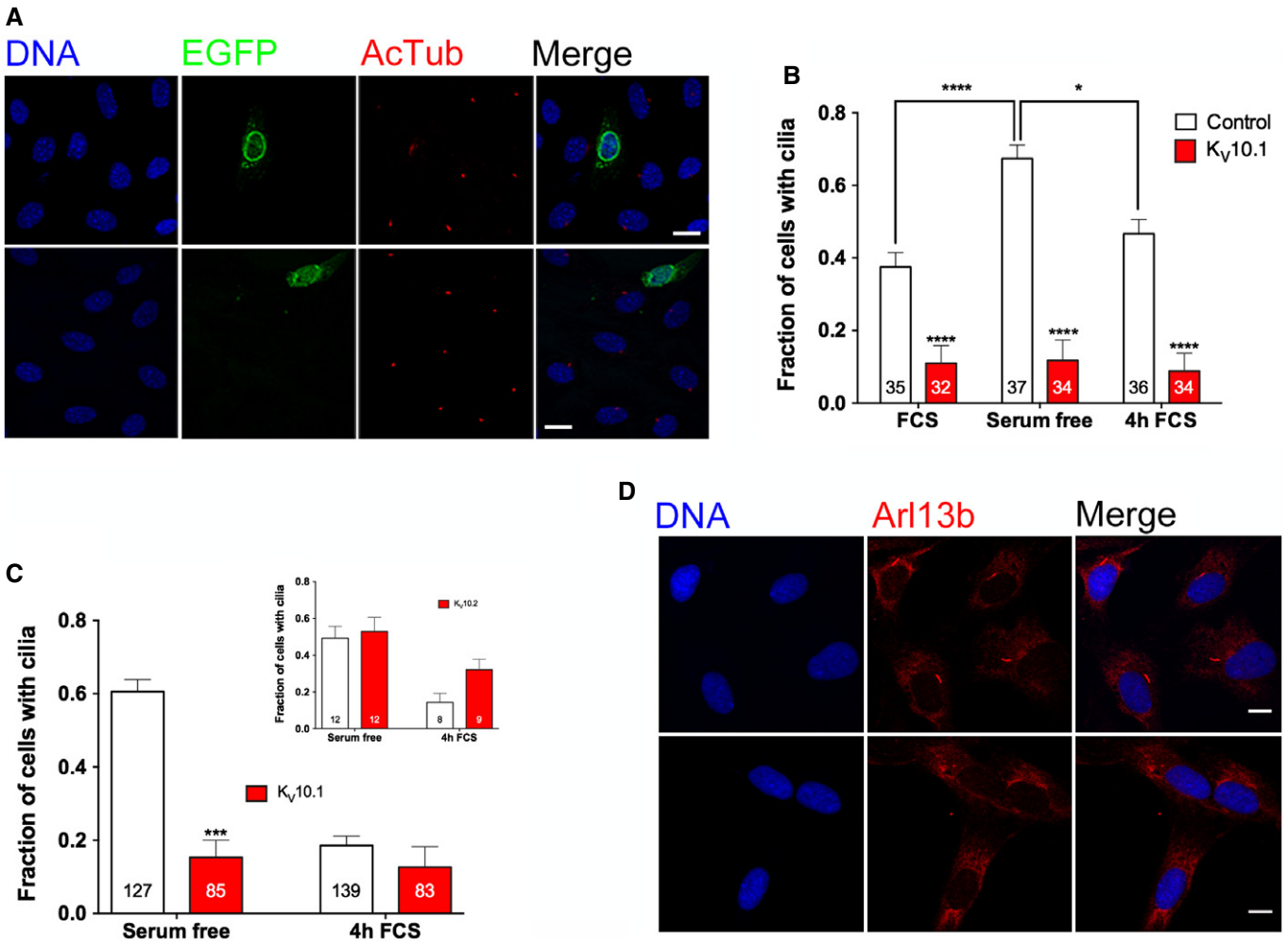

Figure 1. K_V10.1 overexpression impairs ciliogenesis.

A NIH3T3 cells transfected with K_V10.1-EGFP did not show primary cilia. Cells were transiently transfected, after 24 h serum was removed for additional 24 h to induce ciliogenesis, and finally cells were stained with anti-acetylated α-tubulin. While most cells were ciliated, those showing green fluorescence were devoid of cilia. Scale bar: 10 μm.

B NIH3T3 cells transfected with K_V10.1 (red bars) showed markedly less cilia than control cells (empty vector, white bars). Subconfluent cultures grown in the presence of FCS were serum-starved for 24 h to induce ciliogenesis. Cilia were stained with anti-acetylated α-tubulin antibody. To determine ciliary disassembly, cells were starved for 24 h and then incubated for 4 h in FCS to induce cell cycle reentry and ciliary resorption.

C Similarly, hTERT-RPE1 cells transfected with K_V10.1 also showed less cilia. Ciliogenesis and ciliary disassembly were induced as in (B), and cilia were stained using anti-acetylated α-tubulin as in (A) and quantified. The inset shows the equivalent experiment using the structurally related potassium channel K_V10.2, which did not alter the frequency of expression of cilia.

D Examples of fields of view of hTERT-RPE1 cells transfected with K_V10.1, serum-starved for 24 h and cilia revealed with anti-Arl13B antibody (arrows). A majority of control-transfected cells showed cilia, while K_V10.1 transfected did not. Scale bar: 10 μm.

Data information: Data are presented as mean ± SEM. *$P < 0.05$, ***$P < 0.001$, and ****$P < 0.0001$ (two-way ANOVA).

significantly stronger for KO MEFs and most intensely in the case of (besides *Gli1*) *Hhip* and *Ptch1* (Fig EV6). Altogether, our data indicate that the SHH pathway is hyperactive in K_V10.1 knockout MEFs.

Since K_V10.1 is implicated in cell cycle progression [1,40], induction of ciliogenesis by channel knockdown could be secondary to cell cycle arrest. Flow cytometry DNA/RNA measurements with acridine orange [41] revealed that one-half of the cells are in G0 after 24-h serum starvation, and approximately 60% of the cells were ciliated, reflecting again the coupling between ciliogenesis and cell cycle exit. In contrast, in the presence of serum, K_V10.1 knockdown increased the fraction of ciliated cells from 18 to 44%, while the fraction of cells in G0 only increased from 0.5 to 10% (Fig 4A). Therefore, the increase in the fraction of cells in G0 induced by K_V10.1 knockdown was not enough to explain the frequency of ciliated cells, and therefore, a significant fraction of ciliated cells must have left G0. This result suggests that K_V10.1 knockdown reduces the coupling between ciliogenesis and cell cycle.

This could imply that upon K_V10.1 knockdown, ciliated cells can leave G0 before cilia resorption takes place. In control cells, double immunolabeling with the cell proliferation marker Ki-67 and acetylated tubulin to detect cilia revealed that, as expected, most

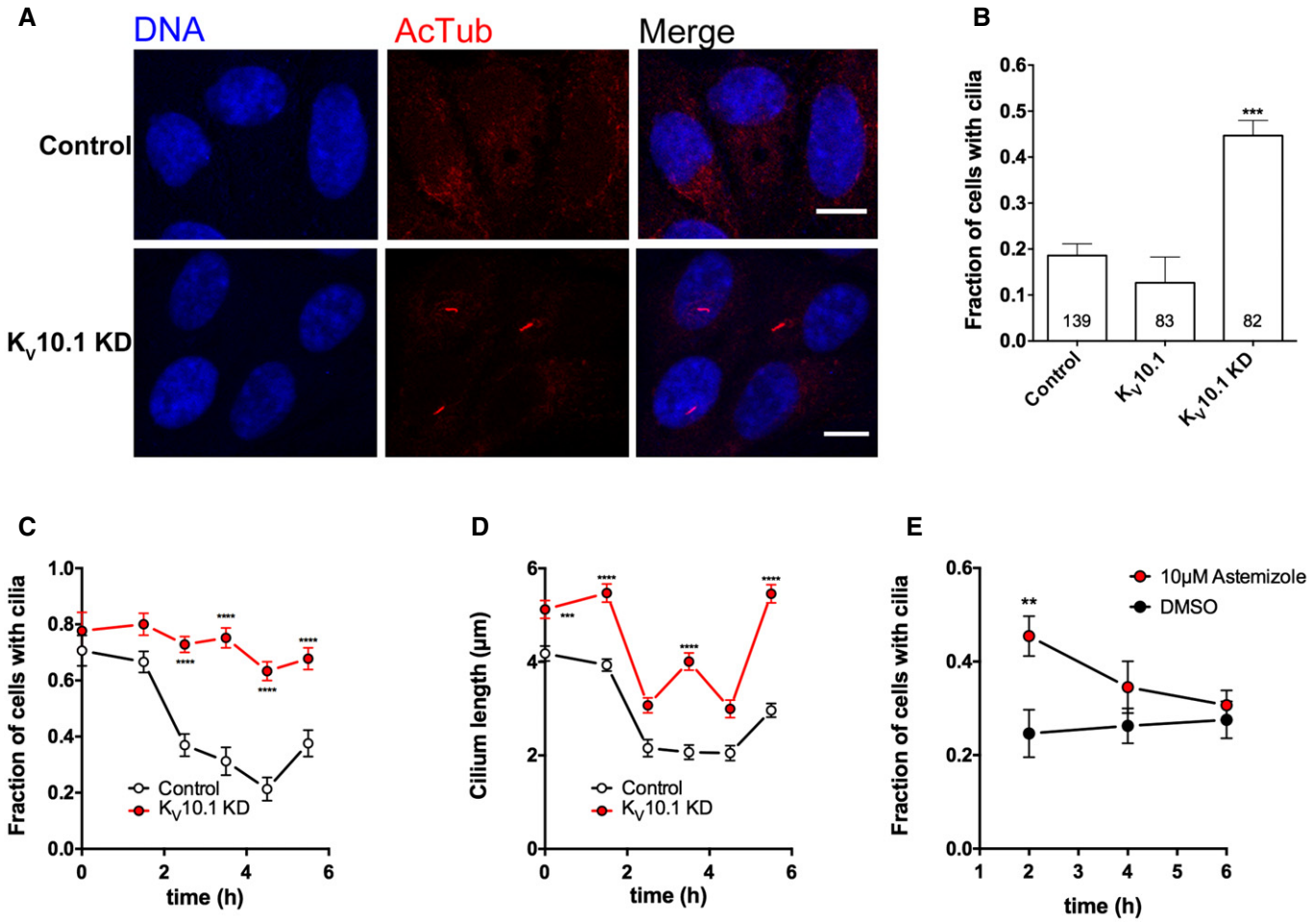

Figure 2. K_V10.1 knockdown induces ciliogenesis.

A Representative images showing hTERT-RPE1 grown in the presence of serum and stained with anti-acetylated α-tubulin antibody. There were more ciliated cells after treatment with siRNA against K_V10.1 (K_V10.1 KD), as compared to scrambled siRNA-transfected cells, which were devoid of cilia (control). Scale bar: 10 µm.

B Quantification of the effect depicted in (A) for the number of images indicated at the base of the columns.

C Time course of ciliary disassembly. hTERT-RPE1 cells were serum-starved for 24 h, fixed at the times indicated after serum reintroduction, and stained with anti-acetylated α-tubulin to reveal cilia. While in the presence of scrambled siRNA the abundance of cilia decreased rapidly (black line), it remained virtually unchanged in cells where K_V10.1 was knocked down (red). N = 8–13.

D Time course of ciliary shortening after serum reintroduction. In the same experiments as in (C), the length of the remaining cilia was measured automatically using ImageJ (FIJI). While ciliary length decreased with a similar time course in the siRNA-treated cells as in controls, cilia were longer in K_V10.1-knockdown cells. A re-elongation of cilia was evident in both populations after 6 h. Numbers of analyzed cilia were between 62 (control, 4.5 h) and 308 (both groups, 1.5 h).

E Blockade of permeation through the K^+ channel altered the speed of deciliation. After serum starvation, medium containing serum and astemizole (10 µM) was added, and cells were fixed and stained at the indicated time points (N = 12).

Data information: Data are presented as mean ± SEM. $^{**}P < 0.01$, $^{***}P < 0.001$, and $^{****}P < 0.0001$ (two-way ANOVA).

(approximately 80%) Ki-67-positive cells were not ciliated. K_V10.1 siRNA reduced the fraction of Ki-67-positive cells by approximately 20%, but it also significantly increased the percentage of Ki-67-positive cells that were at the same time ciliated (Fig 4B and C). The use of an alternative method to label proliferating cells, EdU incorporation, led to similar observations. After K_V10.1 knockdown, many cells were double positive for primary cilia and EdU (Fig 4D), while cells treated with scrambled siRNA were either positive to EdU or ciliated, as also described by others [42]. Taken together, these data indicate that K_V10.1 affects ciliogenesis independently of the effects of the channel on cell cycle, since K_V10.1 knockdown causes a loss of coordination between ciliogenesis and G0/G1 progression, such that ciliated cells can proceed into the cell cycle, in a similar way as do cells where the actin cytoskeleton has been destabilized [43].

K_V10.1 localizes to the primary cilium

We next tested the localization of K_V10.1 in ciliated cells. K_V10.1 localizes to the plasma membrane of neurons and cancer cells, but it is also found to be associated with intracellular structures, including the inner nuclear membrane [44] and endocytic vesicles [21]. However, the localization of the channel had always been studied in actively proliferating (i.e., non-ciliated) cells. To fill this gap, we used human foreskin fibroblasts (HFF), which display a large ciliary

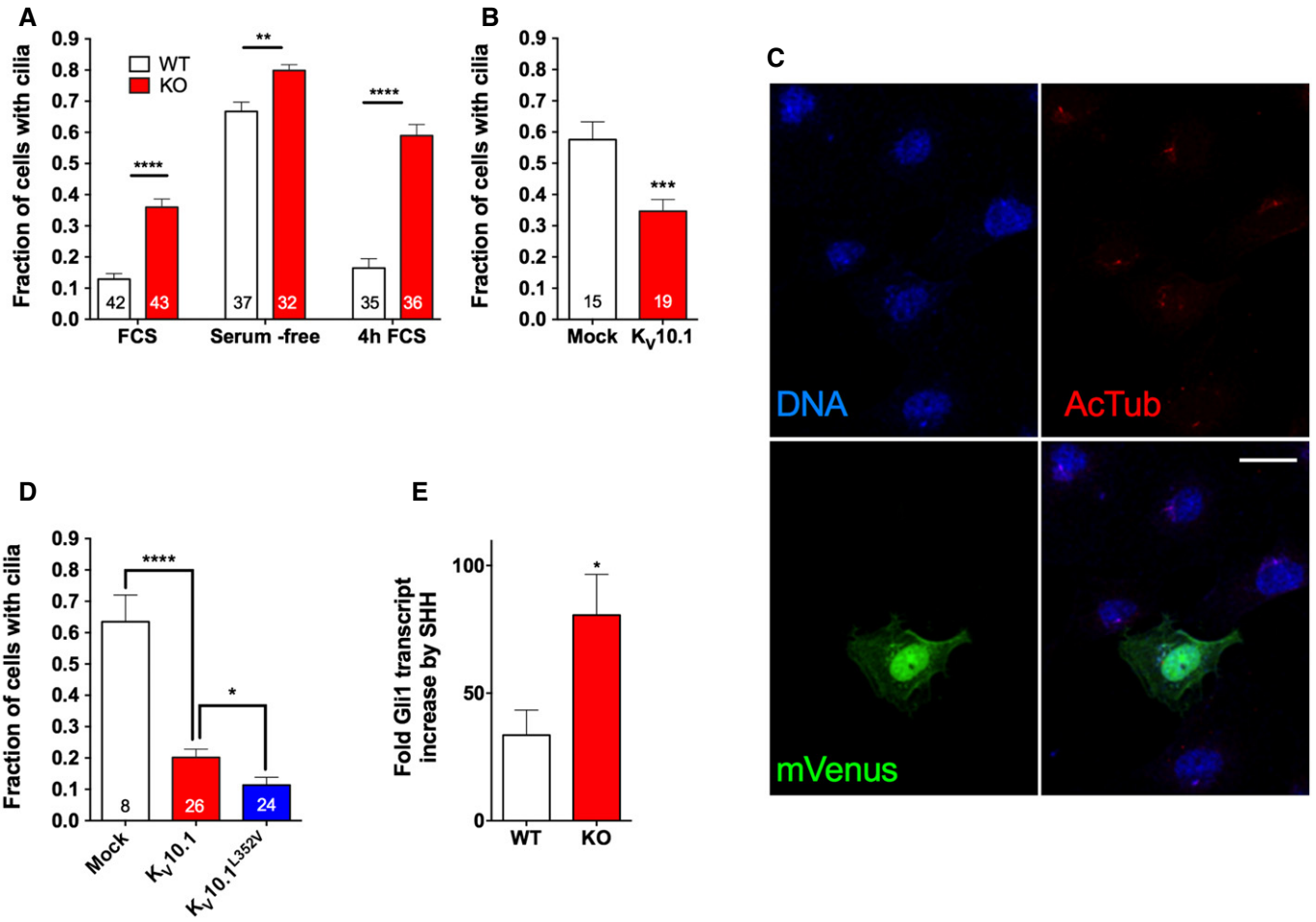

Figure 3. Lack of K_V10.1 increases the fraction of ciliated cells in primary culture from knockout mice.

A Quantification of the amount of ciliated cells in primary embryonic fibroblasts from K_V10.1 knockout mice. Actively growing cultures, cultures after 24-h serum starvation, and 4 h after subsequent serum reintroduction were stained for the presence of cilia using anti-acetylated α-tubulin. An increase in frequency of cilia in the knockout cells was evident under all conditions, but especially marked in the ciliary resorption test (4 h after serum reintroduction), indicating an influence of K_V10.1 expression on deciliation.

B Exogenous expression of human K_V10.1 reverted the phenotype in MEFs. Cells obtained from three animals were transfected with K_V10.1 or empty vector (mock), serum-starved for 48 h, and cilia were revealed by immunocytochemistry using anti-acetylated α-tubulin in the indicated number of images. K_V10.1 expression decreased the frequency of ciliated cells.

C MEFs from knockout mice did not show primary cilia when transfected with K_V10.1. Cells were co-transfected with human K_V10.1 and mVenus, serum-starved for 48 h and then fixed and stained for cilia (AcTub). Venus-positive cells did not show cilia. Scale bar: 25 μm.

D In wild-type MEFs, transfection with K_V10.1 reduced the presence of primary cilia. When a gain-of-function mutant (L352V) that originates developmental defects in human patients was transfected, the frequency of cells with cilia was further reduced.

E Sensitivity to SHH signaling was significantly increased in primary fibroblasts from K_V10.1 knockout mice, in agreement with the higher abundance of primary cilia. Cells were serum-starved, and SHH was stimulated for 48 h by addition of culture supernatant of SHH-expressing HEK293 cells. Expression of mRNA for Gli1 was used as reporter of SHH activation by qRT–PCR.

Data information: Data are presented as mean ± SEM. *P < 0.05, **P < 0.01, ***P < 0.001, and ****P < 0.0001 (A–D, two-way ANOVA; E, non-paired t-test).

pocket [45]. We starved HFF for 24 h to induce ciliogenesis and stained them with an antibody against an extracellular epitope of K_V10.1 and a centrosomal marker (pericentrin) or Arl13B. In these experiments, the anti-K_V10.1 antibody stained elongated structures whose base was pericentrin-positive, as well as Arl13B-positive structures highly suggestive of primary cilia (Fig 5A).

K_V10.1 expression is not constant in all phases of the cell cycle [1]. To increase the fraction of cells expressing K_V10.1, hTERT-RPE1 cells that had been starved for 24 h were stimulated with FCS for 4 h to reinitiate the cell cycle. Immunostainings were then performed with a mixture of monoclonal anti-K_V10.1 antibodies directed against an extracellular epitope [46] and a rabbit monoclonal anti-acetylated α-tubulin. Figure 5B shows that K_V10.1 staining using monoclonal antibodies localizes to a discrete region at the edge of the cilium that is devoid of acetylated microtubules.

Similar experiments were performed on MEFs from wild-type or K_V10.1 knockout mice. The monoclonal antibody used (mAb62) did not stain cells from the knockout animals, confirming specificity (Fig 5C), nor any evident para-ciliar structures (Fig 5D), but did recognize areas close to and at the primary cilium in wild-type MEFs (Fig 5E).

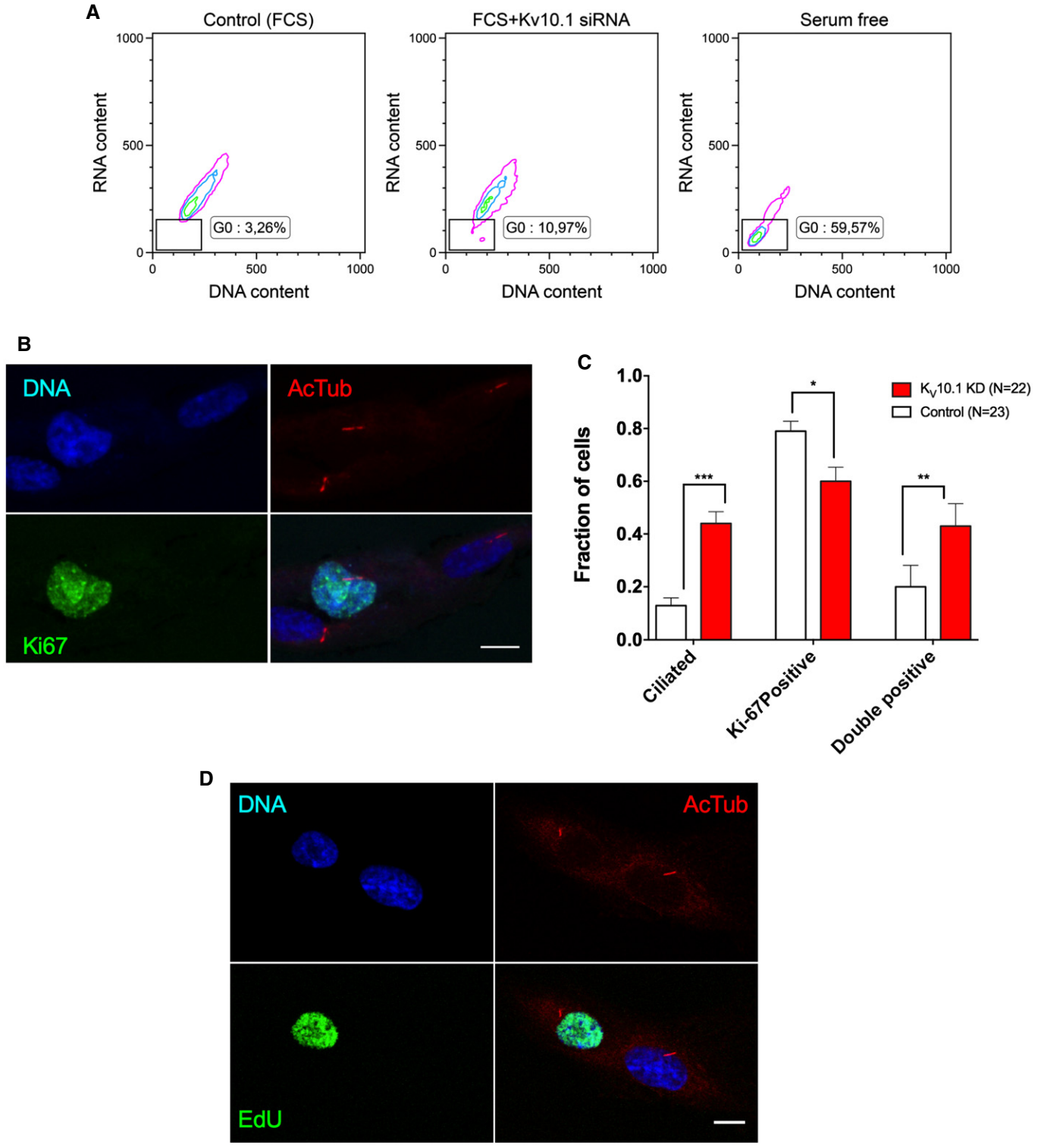

Figure 4.

K_V10.1 is localized in centrosomes

The structures observed in Fig 5B are reminiscent of the pericentrosomal preciliary compartment (PCC) described by [17], which hosts ciliary membrane proteins. When we performed stainings with an anti-K_V10.1 antibody of hTERT-RPE1 (Fig 6A) that had been serum-starved for 48 h and then allowed to resume the cell cycle by reintroduction of serum for 2 h, K_V10.1 colocalized with pericentrin, a centrosomal marker. We observed similar pericentrin-positive structures in cells transfected with a construct that encodes the full-length K_V10.1 fused to a C-terminal fluorescent reporter, under the control of the endogenous promoter of

Figure 4. The effect of K_V10.1 knockdown on ciliogenesis does not obey solely to cell cycle retardation.

A Actively proliferating hTERT-RPE1 cells were transfected with scrambled or K_V10.1 siRNA, and cell cycle distribution was determined using acridine orange staining. Knockdown of K_V10.1 induces an increase in cells with DNA/RNA content compatible with G0 (rectangle). However, the quantitative increase (to approximately 10%) was insufficient to explain the abundance of ciliated cells (over 40%)

B The proliferation marker Ki-67 frequently coexists with primary cilia in K_V10.1-knockdown cells. Exponentially growing cells were stained for acetylated α-tubulin (red, AcTub) and Ki-67 (green). Nuclei were counterstained with Draq5 (blue). Scale bar: 10 μm.

C Quantification of the effects observed in (B). Although the positivity for Ki-67 (proliferating cells) and the presence of cilia were not always excluding each other even in cells transfected with control siRNA, K_V10.1 knockdown increased the frequency of ciliated cells, while it reduced the amount of Ki-67-positive, actively proliferating cells. Of those cells presenting a cilium, the fraction of simultaneously Ki-67-positive cells was much larger upon K_V10.1 knockdown.

D Primary cilia were present in cells actively synthesizing DNA (measured by EdU incorporation). Cells were transfected with siRNA against K_V10.1 and 24 h later were incubated in the presence of EdU for 4 h before fixation. K_V10.1 knockdown resulted in the presence of abundant EdU-positive and simultaneously ciliated cells, suggesting a decoupling between deciliation and cell cycle progression. Scale bar: 10 μm.

Data information: Data are presented as mean ± SEM. $*P < 0.05$, $**P < 0.01$, and $***P < 0.001$ (two-way ANOVA).

K_V10.1, which therefore only drives a mild overexpression of the tagged channel (Fig 6B).

To validate the localization of endogenous K_V10.1 at the centrosomes, we purified centrosomes in density gradient centrifugation experiments; Western blot using a polyclonal anti-K_V10.1 antibody (Fig 7A) revealed a band of the expected size in those fractions that were also positive for centrosomal markers such as Aurora A (phosphorylated or not) and γ-tubulin. There was no co-sedimentation with a cytosolic marker (14-3-3β), and there was also no detectable K_V10.1 signal in fractions positive for transferrin receptor, a plasma membrane marker. The lack of detectable signal in the plasma membrane fractions can be attributed to dilution of K_V10.1 at this location. When the cytoplasmic fraction was ultracentrifuged to sediment the microsomal compartment and concentrate membranes, immunoblot detected K_V10.1 also in the microsomes (Fig 7B). Immunoprecipitation using a mouse antibody different from the rabbit polyclonal used for immunoblot gave positive signals in both the microsomal and the centrosomal fractions (Fig 7B, lanes labeled IP). Importantly, the Western blot revealed that the detected band in the centrosomal fraction has a size that corresponds to full-length K_V10.1, which is expected to be a transmembrane protein.

The ciliary localization signal is required for K_V10.1-induced changes in ciliogenesis and for tumorigenesis

It is well established that targeting of proteins to the primary cilium shares mechanism with nucleo-cytoplasmic transport. In particular, targeting of proteins to the primary cilium implicates the same signals involved in nuclear import/export, including the participation of importins [47]. Consistent with the targeting of K_V10.1 to the cilia, its C-terminus carries a canonical nuclear localization signal [44], predicted to bind to α-importin (using NLS mapper [48]; Fig 8A). We therefore wondered whether this sequence functions as a ciliary localization signal (CLS). Deletion of this sequence ($K_V10.1^{\Delta CLS}$) did not abolish the electrophysiological activity of K_V10.1 (Fig 8B and C). cRNA encoding the mutant channel gave rise to voltage-gated potassium currents (Fig 8C) similar to wild-type K_V10.1 when injected into *Xenopus* oocytes.

In immunocytochemical experiments, we found no evidence of colocalization of $K_V10.1^{\Delta CLS}$ with primary cilia. Consistently, overexpression of $K_V10.1^{\Delta CLS}$ was not able to reduce the fraction of NIH3T3 or hTERT-RPE1 ciliated cells upon serum starvation and subsequent serum reintroduction (Fig 8D).

K_V10.1 expression is known to promote tumor growth, but the process is mechanistically unclear. Prompted by our observations above, we hypothesized that the role in ciliogenesis could underlie the implication of K_V10.1 on tumorigenesis. If this were the case, impairment of the effects on ciliary resorption by deletion of the CLS would also influence tumorigenesis. We previously showed that implantation into the flank of nude mice of CHO K1 cells overexpressing K_V10.1 induced the generation of tumors [23]. CHO K1 cells expressing the $K_V10.1^{\Delta CLS}$ mutant caused smaller tumors than wild-type K_V10.1 expressing cells (Fig 8E). This indicates that the K_V10.1 nuclear localization signal, which is essential for cilia resorption (but not for ion permeation), is also required to mediate tumorigenesis.

Rescue of the effect of K_V10.1 knockdown by activation of cortactin

We have previously reported that K_V10.1 interacts physically with cortactin (CTTN) *in vivo* [22] via its C-terminus. CTTN is required for the correct plasma membrane localization of the channel in proliferating (non-ciliated) cells. CTTN is directly implicated in tumor cell invasion (e.g., [49]), but it also inhibits ciliogenesis [50]). We therefore tested whether the actions of K_V10.1 on ciliary resorption are mediated through its interaction with CTTN. Overexpression of CTTN counteracted the effect of K_V10.1 knockdown on ciliary resorption (Fig 9A), indicating that CTTN participates in the control of ciliogenesis exerted by K_V10.1. Furthermore, overexpression of a K_V10.1 mutant where the residues responsible for interaction with CTTN had been deleted ($K_V10.1^{\Delta 705–755}$) did not affect the fraction of cells showing cilia (Fig 9B).

Importantly, the levels of phosphorylated (active) CTTN were increased in MEFs from K_V10.1 knockout mice, as compared to wild-type mice (Fig 9B), indicating that CTTN can compensate the absence of K_V10.1.

Taken together, our results suggest a temporally restricted cross talk between K_V10.1 and CTTN that appears to be required for the correct disassembly of the primary cilium prior to mitosis.

Discussion

In this paper, we describe a role of the voltage-gated potassium channel K_V10.1 in stimulating primary cilia disassembly. We propose K_V10.1 as a regulator of ciliogenesis, based on its

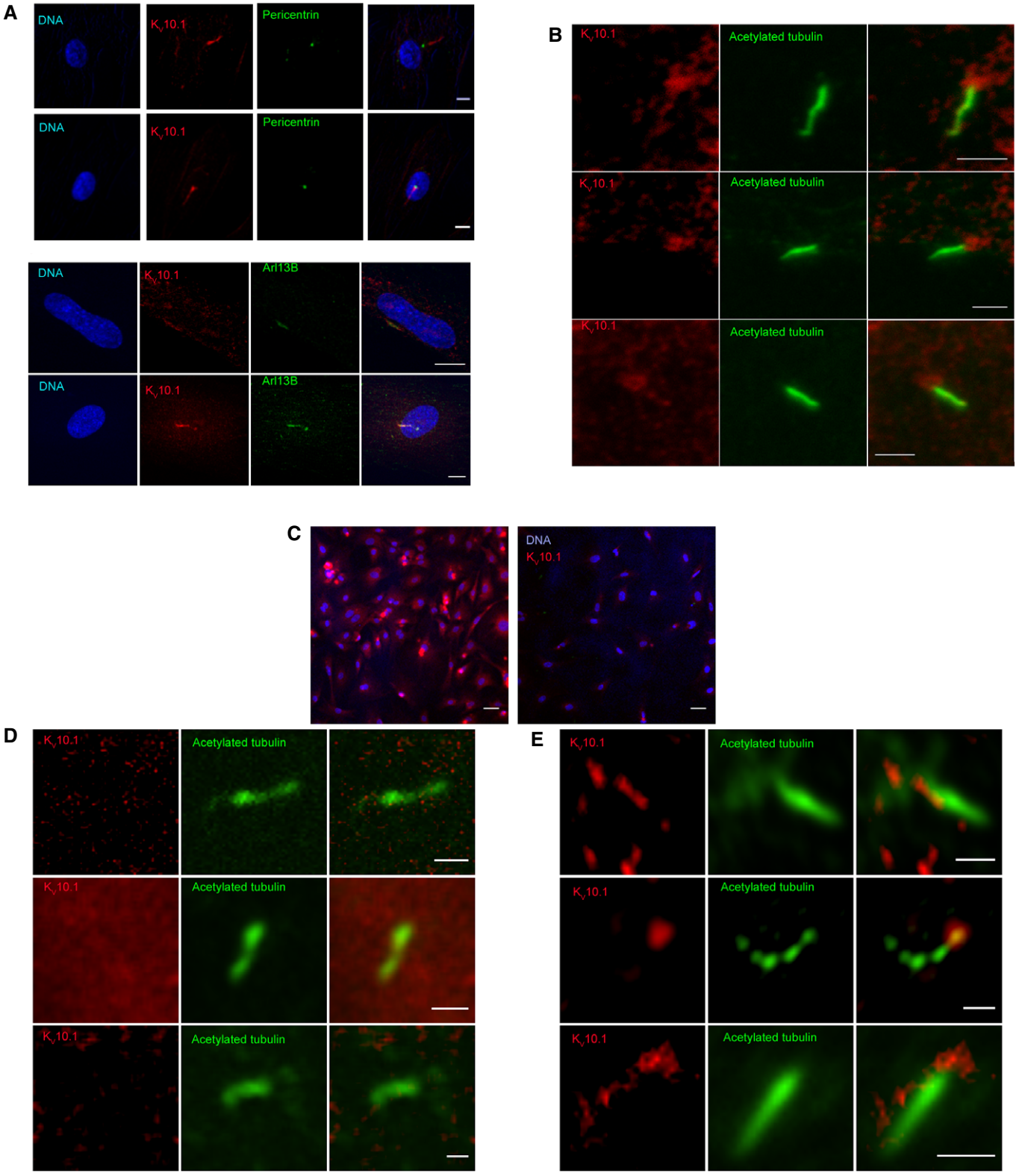

Figure 5.

subcellular localization and the impact that manipulation of its expression has on ciliation in multiple cell types. Work form our group indicates that extra-cerebral expression of K_V10.1 occurs not only in tumor cells, but also in normal cells shortly during G2/M phases in the cell cycle [1], which coincides with the time of disassembly of primary cilia [14].

Figure 5. Localization of K_V10.1 to the primary cilium.

A An anti-K_V10.1 antibody directed against an extracellular epitope labels a structure related to the centrosome (pericentrin-positive) and positive for Arl13b with an appearance suggestive of the primary cilium in HFF (human foreskin fibroblast) cells. Cells were serum-starved for 24 or 48 h, fixed, blocked (10% BSA), and then stained without permeabilization with anti-K_V10.1 antibody recognizing an extracellular epitope. Immunostaining for pericentrin was performed after subsequent permeabilization and additional block. Scale bars: 10 μm (pericentrin), 20 μm (Arl13b).

B Anti-K_V10.1 antibodies recognize ciliary structures in hTERT-RPE1 cells. After serum starvation for 48 h, serum was reintroduced for 4 h to induce K_V10.1 expression and ciliary resorption. Cells were then fixed and stained with a mixture of anti-K_V10.1 mouse monoclonals and a rabbit monoclonal anti-acetylated α-tubulin. Scale bar: 2 μm.

C Specificity of the monoclonal anti-K_V10.1 (mAb 62) as revealed by staining MEFs from wild-type (left) or knockout animals (right). Scale bar: 50 μm.

D Images from primary cilia of MEFs from K_V10.1 knockout mice obtained using mAb62 and a rabbit polyclonal anti-acetylated α-tubulin antibody. No recognizable structures were stained by mAb62. Scale bar: 1 μm.

E In contrast, mAb62 did stain ciliary-related structures (acetylated-tubulin-positive) in wild-type mice. Scale bar: 1 μm.

The functional role of K_V10.1 in ciliogenesis is firstly suggested by the dramatic alteration in the frequency of expression of cilia upon modification of the levels of K_V10.1. Knockdown of K_V10.1 markedly slowed down ciliary resorption after reinitiation of the cell cycle (Fig 2), and primary fibroblasts of K_V10.1 knockout mice produced more cilia than wild type (Fig 3). Conversely, overexpression of K_V10.1 reduced the frequency of ciliated cells (Fig 1).

Additionally, the localization of K_V10.1 also suggests a role in ciliary physiology. K_V10.1 is associated with the centrosome and the primary cilium. We observed that K_V10.1 immunofluorescence colocalizes with pericentrin (Fig 6) shortly after cells reenter the cell cycle. Density gradient fractionation of cell extracts shows that K_V10.1 co-sediments with the centrosomal fraction (Fig 7).

Because the centrosome is a cytosolic organelle, it would be an unexpected location for an integral membrane protein, but the size of the centrosomal K_V10.1 corresponds to the one found in membrane fractions (Fig 7B) and therefore to the full-length protein rather than a fragment. There are several circumstances when centrosomes are tightly associated with membranes that could host K_V10.1 protein. The channel could be targeted to the residual ciliary membrane vesicle that segregates together with the mother centriole during cell division [51]. Alternatively, K_V10.1 could be embedded in the membranes of vesicles at the PCC compartment described in [17] after treatment with cytochalasin D. This could be the reason of the remarkable abundance of K_V10.1 in the centrosomal preparations, which are obtained from cytochalasin-treated cells. In this case, the channel would be associated with the PCC.

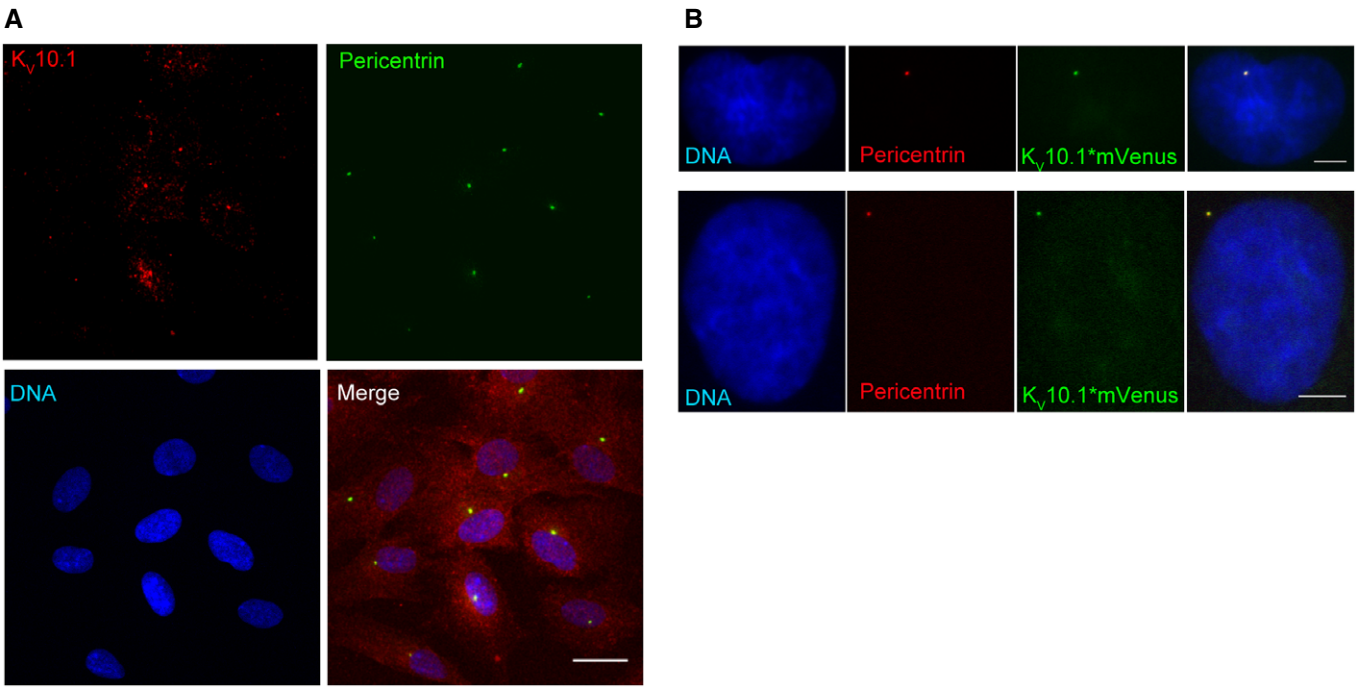

Figure 6. Expression of K_V10.1 at the centrosome.

A K_V10.1 localizes to pericentrin-positive structures during ciliary resorption. After short (4 h) reintroduction of FCS in serum-starved hTERT RPE1 cells, the signal of anti-K_V10.1 antibody colocalized with pericentrin. Scale bar: 25 μm.

B Cells expressing a K_V10.1-mVenus fusion under the control of the endogenous promoter to render a mild overexpression were fixed and immunostained for pericentrin. Venus fluorescence colocalized with pericentrin-positive structures. Scale bar: 5 μm.

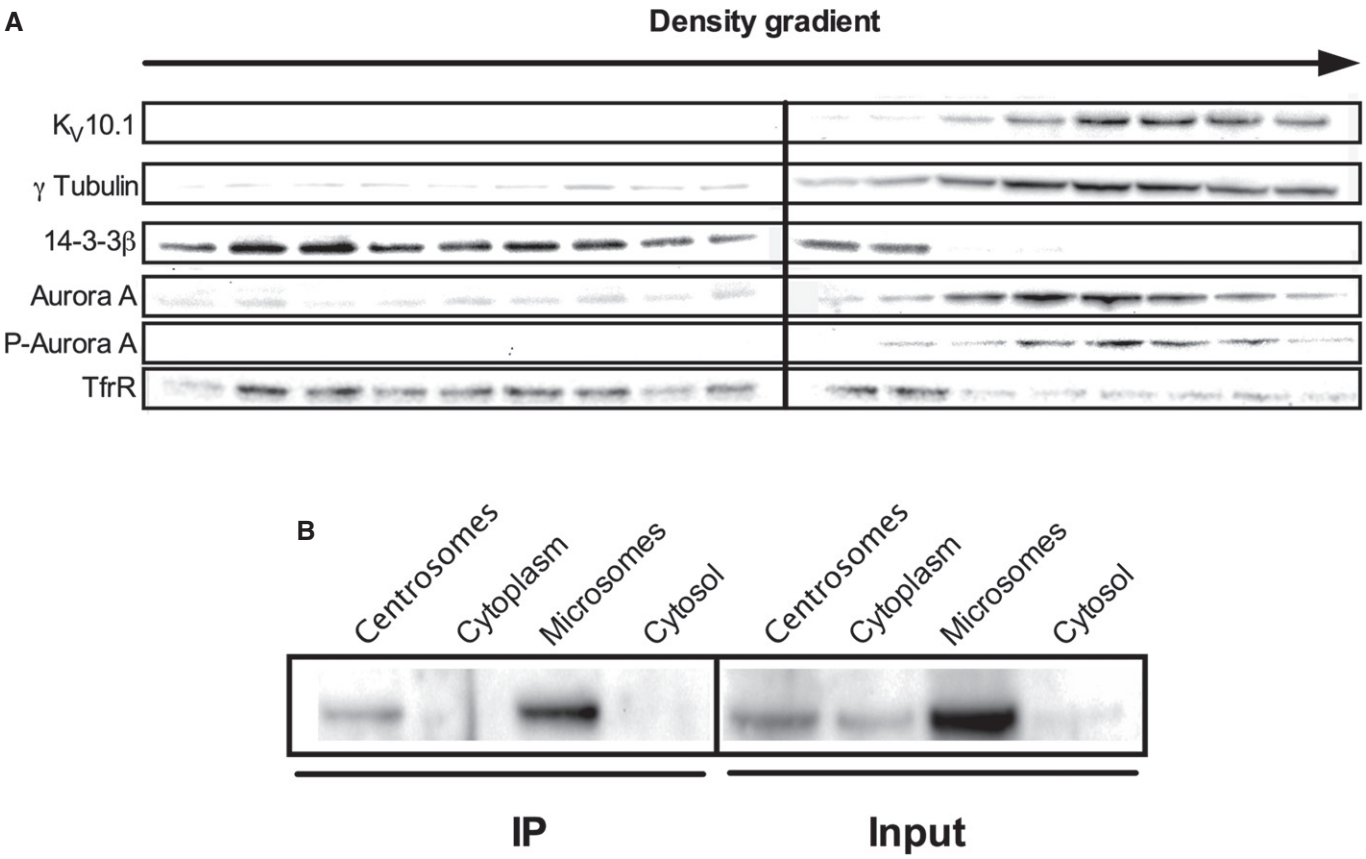

Figure 7. K_V10.1 co-purifies with centrosomes.

A Density gradient centrifugation of hTERT-RPE1 cell extracts followed by immunoblot revealed the presence of K_V10.1 in the same fractions as Aurora A, phospho-Aurora A, and γ-tubulin (centrosomal fractions).

B K_V10.1 is also present in microsomal fractions. Cytoplasmic fractions obtained as in (A) were ultracentrifuged to sediment membranes. In those preparations, immunoprecipitation revealed the presence of full-length K_V10.1 in both the centrosomal and the microsomal fractions (obtained by ultracentrifugation).

Source data are available online for this figure.

A requisite for both alternatives is that the channel is actually associated with the primary cilium while the cell is ciliated. K_V10.1 has been detected in the plasma membrane [52–54], the inner nuclear membrane [44], and intracellular vesicles [21]. Besides those locations, immunofluorescence in ciliated cells detected the channel close to the edge of the primary cilium (Fig 5B and E), and in HFF cells, which show a large ciliary pocket, an elongated structure stemming from the centrosome and Arl13B-positive was detected (Fig 5A).

K_V10.1 is required for normal ciliary resorption when the cell cycle is reinitiated. Inhibition of permeation through the channels (Fig 2E) or reduction in the abundance (Fig 2) or absence of the protein (Fig 3) all impair deciliation. Additionally, a putative CLS in the C-terminus of K_V10.1 appears to be required to induce disassembly of the primary cilium (Fig 8). Importantly, the role of K_V10.1 in inducing ciliary resorption appears to be relevant for the action of the channel in tumorigenesis, because the deletion of the CLS reduces the oncogenicity of transfected cells as compared to cells transfected with the wild-type channel (Fig 8).

If K_V10.1 is implicated in ciliary resorption, one would speculate a developmental phenotype in the presence of channel hyperactivity related to impaired ciliogenesis. This is indeed the case for Temple–Baraitser and Zimmermann–Laband syndromes, recently identified as gain-of-function mutations in K_V10.1 [24,25]. Both diseases show orofacial and digital abnormalities (together with severe mental retardation), and their morphological features are highly reminiscent of ciliopathies. Indeed, expression of a mutant identified in Zimmermann–Laband patients exacerbated the effect of K_V10.1 on ciliary resorption.

There are several alternatives to explain mechanistically the action of K_V10.1 on deciliation. Given that K^+ permeation is required, the effect should be associated with local hyperpolarization of the membrane, which would have several effects. First, it would increase the driving force for Ca^{2+} entry, a phenomenon that has been long known to be important for deciliation [55]. Additionally, local changes in potential would influence the phospholipid composition of the membrane [56]; more specifically, it would reduce nanoclustering of PIP_2, which influences the competence of the permeation barrier at the transition zone of the primary cilium [57]. Interestingly, a recent report noticed that another voltage-gated potassium channel (K_V7.1, *KCNQ1*) has the opposite effects in the mouse kidney [58], because its absence impairs ciliogenesis,

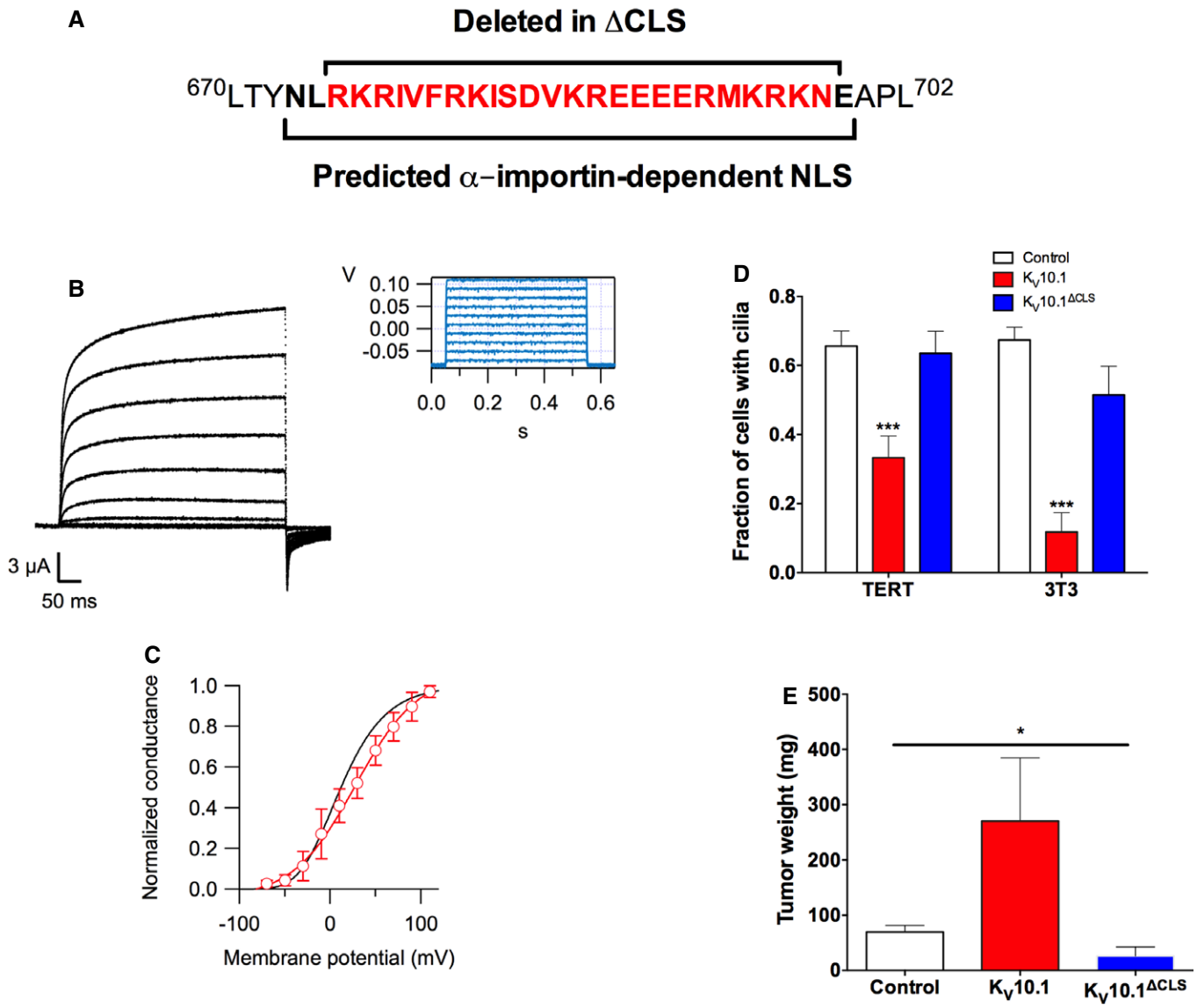

Figure 8. The CLS sequence in the C-terminus of K_V10.1 is required for accelerating deciliation.

A C-terminal amino acid sequence of K_V10.1, indicating the predicted importin-α recognition sequence (bold) and the deleted fragment n $K_V10.1^{\Delta NLS}$ (red).

B Deletion of the CLS does not preclude functional expression at the plasma membrane. Two-electrode voltage-clamp recordings from *Xenopus* oocytes injected with cRNA for a K_V10.1 channel lacking the CLS at the C-terminus revealed voltage-gated currents after stimulation using the potential depicted in the inset. The conductance/voltage relationship of the deleted channel was similar to that of wild type (shown for comparison as a solid line).

C In the absence of serum, the C-terminus of K_V10.1 reduced the number of cilia (maintained cells deciliated) also after deletion of the CLS (data for controls are reproduced from Fig 5A)

D The CLS is required to induce deciliation. When hTERT-RPE1 and 3T3 cells transfected with K_V10.1 or $K_V10.1^{\Delta CLS}$ were serum-starved, and serum was reintroduced after 24 h for 4 h, $K_V10.1^{\Delta CLS}$ failed to reduce the fraction of ciliated cells.

E The CLS is required for K_V10.1-induced tumorigenesis. CHO cells were transfected with the indicated constructs and implanted into the flank of nude mice. $K_V10.1^{\Delta CLS}$ transfected cells did not induce larger tumors than the control.

Data information: Data are presented as mean ± SEM. *$P < 0.05$ and ***$P < 0.001$ (two-way ANOVA).

indicating that K^+ permeability alone is not responsible for the effects we report here, and that the spatiotemporal control of expression and/or interactions with other proteins are required. Interactions of K_V10.1 with CTTN appear crucial for the regulation of ciliogenesis by the channel (Fig 9). CTTN overexpression has been reported to reduce ciliogenesis, in a similar way as K_V10.1 does [50]. Overexpression of CTTN rescued the effects of K_V10.1 knockdown, suggesting that both proteins share a common pathway. It is known that actin branching has inhibitory effect in ciliogenesis [43], and this would be influenced by CTTN through Arp2/3 [17] and CTTN is also important for centrosomal separation at the G2/M transition. Remarkably, phosphorylated CTTN localizes to the

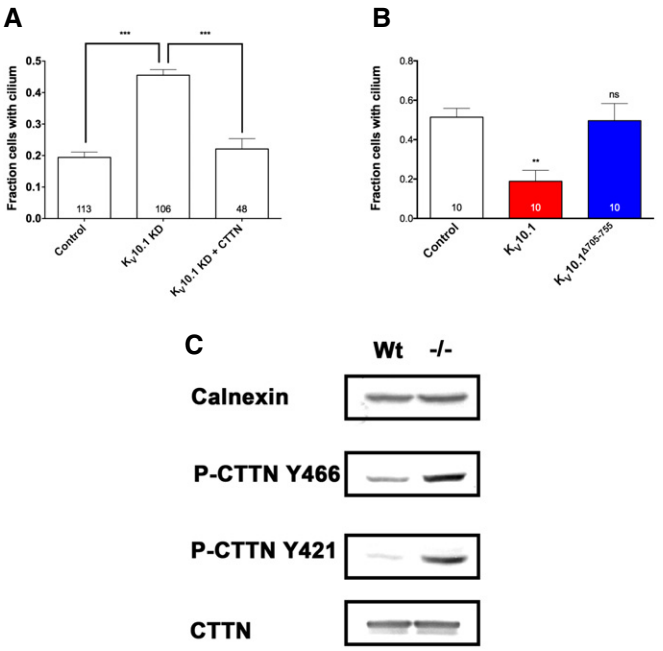

Figure 9. Cross talk with cortactin.

A Overexpression of cortactin compensated for the knockdown of K_V10.1 in ciliary disassembly (4-h serum reintroduction after starvation).

B Deletion of the domain of K_V10.1 responsible for interaction with cortactin abolished the effects of K_V10.1 overexpression on the abundance of cilia.

C In mouse embryonic fibroblasts, active (phosphorylated) cortactin is increased as compared to wild type, possibly compensating the lack of K_V10.1.

Data information: Data are presented as mean ± SEM. $^{**}P < 0.01$ and $^{***}P < 0.001$ (ANOVA).
Source data are available online for this figure.

centrosome [59]. CTTN overexpression is very effective in complementing lack of K_V10.1, and its hyperactivation in knockout MEFs is also compatible with this scenario. Nevertheless, other candidates as mediators of the actions of K_V10.1 on ciliary resorption can at this point not be discarded. Additionally, MEFs from KO mice show alterations in pathways that are related to ciliary structure and function, such as Wnt [60], TGFβ [61], and Hippo [62], and K_V10.1 interacts with additional candidate regulators of ciliogenesis, like RabEP1 [21,63].

Our working hypothesis, in summary, is that the participation of K_V10.1 in ciliary resorption would lead to two types of alterations, depending on the developmental stage. During development, excess activity of K_V10.1 would induce malformations, and in already developed tissues, it would favor tumorigenesis. Taken together, our results prompt for a mechanistic answer for the long sought link between voltage-gated potassium channels and cell proliferation, different from a general or diffuse variation in membrane potential induced by changes in potassium permeability, and involving a more specific participation in the cell biological process itself. Further work should get deeper into the role of local K^+ flow in the process of ciliary disassembly, as it is the case for Ca^{2+} [64]. This has important consequences also when approaching the design of therapy strategies with these channels as targets.

Materials and Methods

Cell culture and lysis

hTERT-RPE1 (ATCC CRL 4000), NIH 3T3 (DSMZ ACC 59), CHO-K1 (DSMZ ACC 110), and HFF (a gift from S. Christensen, University of Copenhagen) cells were grown following the indications of the suppliers. For imaging experiments, cells were grown on glass coverslips. Depending on the particular experiments, cells at approximately 70% confluence were transfected using Lipofectamine siRNAMax, Lipofectamine 2000, Lipofectamine LTX Plus (Thermo Fisher Scientific, Darmstadt, Germany), or nucleofection (Lonza Amaxa, Basle, Switzerland). Imaging experiments were performed 48–72 h after transfection. To induce ciliogenesis, the cells were incubated in serum-free medium for 24 or 48 h, and serum was reintroduced for 4 h to measure cilium disassembly. At the end of the incubation period, cells were washed with TBS and fixed using Accustain (Sigma, Munich, Germany; 8 min at 4°C) and permeabilized with 0.5% Triton X-100 (Calbiochem, Darmstadt, Germany). Non-specific binding sites were blocked with 10% BSA and stained using anti-acetylated α-tubulin (ab24610, Abcam, Cambridge, UK or Rabbit mAb #5335, Cell Signaling Technologies, Danvers, MA), anti-pericentrin (Abcam 4448), Anti-Arl13B (17711-1AP; Proteintech, Chicago, IL), and AlexaFluor 488, Alexa Fluor 546, or AlexaFluor 647 secondary antibodies (Thermo Fisher Scientific). Nuclei were stained with ToPro3 (Thermo Fisher Scientific) or Draq5 (Biostatus, Shepshed, UK).

Ki-67 antibody (556003, Becton Dickinson, Heidelberg, Germany) was used to assess actively proliferating cells. 5-ethynyl-2′-deoxyuridine (EdU) incorporation was determined by incubating cells for 4 h in medium containing 10 μM EdU. The cells were subsequently fixed, permeabilized, and EdU was detected using Click-iT EdU Alexa Fluor 488 imaging kit (Thermo Fisher Scientific) after the recommendations of the manufacturer. The subsequent immunocytochemical staining was performed as described above.

To prepare lysates, cells were washed twice with 4°C PBS, scraped, pelleted at 600 *g* for 5 min, and resuspended in 3 volumes of lysis buffer (50 mM Tris–HCl pH 7.4, 300 mM NaCl, 5 mM EDTA, 1% Triton X-100, with cOmplete protease inhibitor (Roche Applied Science, Mannheim, Germany). After 15 min on ice, the lysate was cleared by centrifugation (15 min, 14,000 *g*, 4°C). Finally, the supernatant was homogenized through a 0.45-mm needle. Protein concentration was determined by BCA (Thermo Fisher Scientific); samples were stored at −70°C.

For assessing SHH activity, cells were serum-starved for 48 h and stimulated with a culture supernatant of HEK293 cells expressing human SHH (a gift from H. Hahn, University of Göttingen) in 0.5% FCS. The cells were subsequently harvested, and the abundance of Gli1 mRNA was measured by qRT–PCR.

Centrosomal purification

hTERT-RPE1 cells were treated with cytochalasin D (1 μg/ml) and nocodazole (0.2 μM) for 1 h. Cytochalasin D promotes ciliogenesis on its own, but it requires longer periods of time to affect cilia [43]. Cells were then lysed in lysis buffer (1 mM HEPES pH 7.2,

0.5% Nonidet P40, 0.5 mM $MgCl_2$, 0.1% β-mercaptoethanol) supplemented with protease inhibitors. Cell lysates were subjected to gradient centrifugation, and centrosomal fractions were purified using a discontinuous sucrose density gradient centrifugation as described in [65] (40, 50, and 70% sucrose). The fractions were further analyzed by Western blot.

Cell cycle analysis

Acridine orange RNA/DNA differential staining was performed after reference [41]. In brief, cells resuspended in 200 µl PBS + 1% BSA at 1×10^6 cells/ml were permeabilized under acidic conditions (by addition of 0.4 ml 0.1% Triton X-100, 80 mM HCl, 150 mM NaCl) for 15 s and immediately stained by addition of 1.2 ml 37 mM citric acid, 126 mM Na_2HPO_4, 150 mM NaCl, 1 mM Na_2EDTA, and 6 µg/ml acridine orange (Thermo Fisher Scientific). Thereafter, staining was measured in a BD FACS Aria flow cytometer (BD Biosciences, Heidelberg, Germany). AO was excited with the 488-nm laser line, and emission was recorded at 530 nm (DNA) and over 630 nm (RNA). Only single viable cells (as determined by forward–sideward scatter) were gated and further analyzed. Data were analyzed with FlowJo (TreeStar, Ashland, OR) and Kaluza (Beckman-Coulter, Brea, CA) software.

Immunoprecipitation/Western blot

Lysate samples containing 200–600 µg cell were precleared using 25 µl protein G magnetic beads (New England BioLabs, Frankfurt, Germany); after 1-h incubation and removal of the beads, the precleared lysate was incubated with 3 µg mAb33 anti-K_V10.1 antibody for 1 h, and 25 µl clean protein G magnetic beads were added and incubated for 1 h. The recovered beads were then washed with 50 mM Tris–HCl pH 7.4, 300 mM NaCl, 5 mM EDTA, and 0.1% Triton X-100. Bound proteins were eluted with PAGE loading buffer. Samples were separated in 3–8% or 4–12% gradient polyacrylamide precast gradient gels (Thermo Fisher Scientific), transferred to nitrocellulose membranes, and immunoblotted with polyclonal anti-K_V10.1 antibody (9391).

For Western blot of additional proteins, the following antibodies were used: pan-14-3-3 (sc-629, Santa Cruz Biotechnology, Santa Cruz, CA), Actin (I19, Santa Cruz), phospho-Aurora A (#3079, Cell Signaling Technologies, Danvers, MA), Aurora A (#12100; Cell Signaling), Calnexin (ADI SPA 860, Enzo Life Sciences, Lörrach, Germany), Cortactin (ab81208, Abcam), phospho-cortactin (Y466, SAB4504373, and Y421, SAB4504372, both from Sigma), γ-tubulin (sc7396, Santa Cruz), and human transferrin receptor (612125, BD).

Animal experiments

Two million CHO cells transfected with K_V10.1, $K_V10.1^{\Delta CLS}$, or empty vector were injected into the flank of male athymic nude mice (NMRI-Fox1nu/nu) maintained in a sterile environment in special cages with filter huts. The group size was chosen as for [3,23]. Due to the objective nature of the experiment, no randomization or blinding was necessary. Four weeks after implant, the tumors were dissected and weighted. No invasion of surrounding tissues was observed in any case. Animal manipulation was performed in accordance with guidelines of the State of Lower Saxony and the University Medicine Göttingen.

Real-time PCR

Quantitative PCR was performed in a LightCycler 480 (Roche) on cDNA obtained from total mRNA using SuperScript III First-Strand Synthesis System (Invitrogen). SYBRGreen system was used mouse *Gli1* (5′-TACATGCTGGTGGTGCACATG and 5′-ACCGAAGGTGCGTC TTGAGG) and TaqMan probes for K_V10.1 (Primers 5′-TCTGTCCTG TTTGCCATATGATGT, 5′-CGGAGCAGCCGGACAA, and probe: FAM-AACGTGGA-amino C6 dT-GAGGGCATCAGCAGCCT). Housekeeping genes were mouse actin for Gli1 (5′ ATGGATGACGATATCGCTG CGCTGG and 5′ CTAGAAGCACTTGCGGTGCACGATGG), and transferrin receptor for K_V10.1 (primers: 5′ GACTTTGGATCGGTTGGTG C, and 5′-CCAAGAACCGCTTTATCCAGAT, and probe: JOE-TGAAT GGCTAGAGGGA-TAMRAdT-ACCTTTCGTCCC).

Alternatively, an array containing 84 genes involved in SHH pathway and 5 housekeeping genes (RT^2 Profiler PCR Array Mouse Hedgehog Signaling Pathway, cat. PAMM-078Z, Qiagen) was used to detect changes between KO and WT MEFs before (serum-starved) and after SHH stimulation. cDNA from cells in each of the conditions was applied directly to the commercially available plates.

Electrophysiology

Two-electrode voltage-clamp recordings were performed at room temperature 2–5 days after injection of 50 nl cRNA, using a Turbo TEC-10CD amplifier (NPI electronics). The intracellular electrodes had resistances of 0.5–1.0 MΩ when filled with 2 M KCl. The extracellular measuring solution contained 115 mM NaCl, 2.5 mM KCl, 1.8 mM $CaCl_2$, 10 mM HEPES/NaOH, pH 7.2. For recordings in high extracellular K^+, like those used for Fig 8B and C, KCl was increased to 60 mM substituting NaCl.

Data acquisition and analysis were performed with the PulsePulseFit (HEKA Electronics) and IgorPro (WaveMetrics) software packages.

Microscopy

Images were obtained on a LSM 510 Meta confocal laser-scanning microscope with Zen software (both from Zeiss, Göttingen, Germany) at room temperature using an oil-immersion Zeiss Plan Neofluar 63× (NA 1.25) or on a Nikon-Andor spinning disk microscope and NIS software. Fluorochromes are indicated in each image. Only linear corrections and Gaussian blur were applied to the images offline using FIJI [66]. To determine the fraction of ciliated cells, a z-stack spanning the thickness of the cell layer was recorded to detect cilia located at different levels in the preparation. Displayed images correspond to z-projections of the stack.

Statistical methods

All experiments were performed at least three times. At least three biological replicates were evaluated for each experiment. The number of images analyzed for each condition, or when appropriate

the number of independent experiments is indicated in bar diagrams by a number at the base of each bar. Data were analyzed using Prism 6 (GraphPad Software, La Jolla, CA). Non-paired, two-sided Student's *t*-test, one-way ANOVA, or two-way ANOVA were used as appropriate. Unless otherwise stated, all data are reported as mean ± SEM. Asterisks indicate *P* values of < 0.05 (*), < 0.01 (**), < 0.001 (***), and < 0.0001 (****), respectively.

Expanded View for this article is available online.

Acknowledgements
We thank Prof. Walter Stühmer for continued support and critical comments to the manuscript. V. Díaz-Salamanca, K. Dümke, B. Heidrich, M. Kothe, and U. Kutzke provided technical assistance. We thank Prof. F. Alves and Dr. J. Napp (Göttingen) for help with animal experiments; Prof. H. Hahn (Göttingen) for cells overexpressing SHH; Prof. ST Christensen (Copenhagen) for sharing reagents and for helpful suggestions; and Profs. F. Ashcroft (Oxford), M. González-Gaitán (Geneva), F. Fernández de Miguel (Mexico), E. Neher (Göttingen), and S.F. Pedersen (Copenhagen) for comments on the manuscript.

Author contributions
AS, DU, and LAP participated in the design of the study, performed experiments, and analyzed the results. LAP wrote the first version of the manuscript.

Conflict of interest
The authors declare that they have no conflict of interest.

References

1. Urrego D, Movsisyan N, Ufartes R, Pardo LA (2016) Periodic expression of Kv10.1 driven by pRb/E2F1 contributes to G2/M progression of cancer and non-transformed cells. *Cell Cycle* 15: 799 – 811
2. Pardo LA, Stühmer W (2014) The roles of K+ channels in cancer. *Nat Rev Cancer* 14: 39 – 48
3. Downie BR, Sánchez A, Knötgen H, Contreras-Jurado C, Gymnopoulos M, Weber C, Stühmer W, Pardo LA (2008) Eag1 expression interferes with hypoxia homeostasis and induces angiogenesis in tumors. *J Biol Chem* 283: 36234 – 36240
4. Goetz SC, Anderson KV (2010) The primary cilium: a signalling centre during vertebrate development. *Nat Rev Genet* 11: 331 – 344
5. Kobayashi T, Dynlacht BD (2011) Regulating the transition from centriole to basal body. *J Cell Biol* 193: 435 – 444
6. Pan J, Snell W (2007) The primary cilium: keeper of the key to cell division. *Cell* 129: 1255 – 1257
7. Badano JL, Mitsuma N, Beales PL, Katsanis N (2006) The ciliopathies: an emerging class of human genetic disorders. *Annu Rev Genomics Hum Genet* 7: 125 – 148
8. Tobin JL, Beales PL (2009) The nonmotile ciliopathies. *Genet Med* 11: 386 – 402
9. Luijten MNH, Basten SG, Claessens T, Vernooij M, Scott CL, Janssen R, Easton JA, Kamps MAF, Vreeburg M, Broers JLV *et al* (2013) Birt–Hogg–Dubé syndrome is a novel ciliopathy. *Hum Mol Genet* 22: 4383 – 4397
10. Cortés CR, Metzis V, Wicking C (2015) Unmasking the ciliopathies: craniofacial defects and the primary cilium. *Wiley Interdiscip Rev Dev Biol* 4: 637 – 653
11. Brown JM, Witman GB (2014) Cilia and diseases. *Bioscience* 64: 1126 – 1137
12. Spalluto C, Wilson DI, Hearn T (2013) Evidence for reciliation of RPE1 cells in late G1 phase, and ciliary localisation of cyclin B1. *FEBS Open Bio* 3: 334 – 340
13. Wang W, Wu T, Kirschner MW (2014) The master cell cycle regulator APC-Cdc20 regulates ciliary length and disassembly of the primary cilium. *eLife* 3: e03083
14. Pugacheva EN, Jablonski SA, Hartman TR, Henske EP, Golemis EA (2007) HEF1-dependent Aurora A activation induces disassembly of the primary cilium. *Cell* 129: 1351 – 1363
15. Wang J, Deretic D (2014) Molecular complexes that direct rhodopsin transport to primary cilia. *Prog Retin Eye Res* 38: 1 – 19
16. Yoshimura S, Egerer J, Fuchs E, Haas AK, Barr FA (2007) Functional dissection of Rab GTPases involved in primary cilium formation. *J Cell Biol* 178: 363 – 369
17. Kim J, Lee JE, Heynen-Genel S, Suyama E, Ono K, Lee K, Ideker T, Aza-Blanc P, Gleeson JG (2010) Functional genomic screen for modulators of ciliogenesis and cilium length. *Nature* 464: 1048 – 1051
18. Lin H, Li Z, Chen C, Luo X, Xiao J, Dong D, Lu Y, Yang B, Wang Z (2011) Transcriptional and post-transcriptional mechanisms for oncogenic overexpression of ether à go-go K^+ channel. *PLoS ONE* 6: e20362
19. Ren B, Cam H, Takahashi Y, Volkert T, Terragni J, Young RA, Dynlacht BD (2002) E2F integrates cell cycle progression with DNA repair, replication, and G(2)/M checkpoints. *Genes Dev* 16: 245 – 256
20. Zhu W, Giangrande PH, Nevins JR (2004) E2Fs link the control of G1/S and G2/M transcription. *EMBO J* 23: 4615 – 4626
21. Ninkovic M, Mitkovski M, Kohl T, Stühmer W, Pardo LA (2012) Physical and functional interaction of $K_V10.1$ with Rabaptin-5 impacts ion channel trafficking. *FEBS Lett* 586: 3077 – 3084
22. Herrmann S, Ninkovic M, Kohl T, Lörinczi E, Pardo LA (2012) Cortactin controls surface expression of the voltage-gated potassium channel $K_V10.1$. *J Biol Chem* 287: 44151 – 44163
23. Pardo LA, del Camino D, Sanchez A, Alves F, Brüggemann A, Beckh S, Stühmer W (1999) Oncogenic potential of EAG K^+ channels. *EMBO J* 18: 5540 – 5547
24. Kortüm F, Caputo V, Bauer CK, Stella L, Ciolfi A, Alawi M, Bocchinfuso G, Flex E, Paolacci S, Dentici ML *et al* (2015) Mutations in KCNH1 and ATP6V1B2 cause Zimmermann-Laband syndrome. *Nat Genet* 47: 661 – 667
25. Simons C, Rash LD, Crawford J, Ma L, Cristofori-Armstrong B, Miller D, Ru K, Baillie GJ, Alanay Y, Jacquinet A *et al* (2015) Mutations in the voltage-gated potassium channel gene KCNH1 cause Temple-Baraitser syndrome and epilepsy. *Nat Genet* 47: 73 – 77
26. Fukai R, Saitsu H, Tsurusaki Y, Sakai Y, Haginoya K, Takahashi K, Hubshman MW, Okamoto N, Nakashima M, Tanaka F *et al* (2016) De novo KCNH1 mutations in four patients with syndromic developmental delay, hypotonia and seizures. *J Hum Genet* doi:10.1038/jhg.2016.1
27. Seeley ES, Nachury MV (2010) The perennial organelle: assembly and disassembly of the primary cilium. *J Cell Sci* 123: 511 – 518
28. Bodnar AG, Ouellette M, Frolkis M, Holt SE, Chiu CP, Morin GB, Harley CB, Shay JW, Lichtsteiner S, Wright WE (1998) Extension of life-span by introduction of telomerase into normal human cells. *Science* 279: 349 – 352
29. Ju M, Wray D (2002) Molecular identification and characterisation of the human eag2 potassium channel. *FEBS Lett* 524: 204 – 210
30. Ludwig J, Weseloh R, Karschin C, Liu Q, Netzer R, Engeland B, Stansfeld C, Pongs O (2000) Cloning and functional expression of rat eag2, a new member of the ether-à-go-go family of potassium channels and

comparison of its distribution with that of eag1. *Mol Cell Neurosci* 16: 59 – 70

31. Schönherr R, Gessner G, Löber K, Heinemann SH (2002) Functional distinction of human EAG1 and EAG2 potassium channels. *FEBS Lett* 514: 204 – 208
32. Tucker RW, Pardee AB, Fujiwara K (1979) Centriole ciliation is related to quiescence and DNA synthesis in 3T3 cells. *Cell* 17: 527 – 535
33. García-Ferreiro RE, Kerschensteiner D, Major F, Monje F, Stühmer W, Pardo LA (2004) Mechanism of block of hEag1 K^+ channels by imipramine and astemizole. *J Gen Physiol* 124: 301 – 317
34. Li A, Saito M, Chuang J-Z, Tseng Y-Y, Dedesma C, Tomizawa K, Kaitsuka T, Sung C-H (2011) Ciliary transition zone activation of phosphorylated Tctex-1 controls ciliary resorption, S-phase entry and fate of neural progenitors. *Nat Cell Biol* 13: 402 – 411
35. Kowal TJ, Falk MM (2015) Primary cilia found on HeLa and other cancer cells. *Cell Biol Int* 39: 1341 – 1347
36. Ufartes R, Schneider T, Mortensen LS, de Juan Romero C, Hentrich K, Knoetgen H, Beilinson V, Moebius W, Tarabykin V, Alves F *et al* (2013) Behavioural and functional characterization of Kv10.1 (Eag1) knockout mice. *Hum Mol Genet* 22: 2247 – 2262
37. May SR, Ashique AM, Karlen M, Wang B, Shen Y, Zarbalis K, Reiter J, Ericson J, Peterson AS (2005) Loss of the retrograde motor for IFT disrupts localization of Smo to cilia and prevents the expression of both activator and repressor functions of Gli. *Dev Biol* 287: 378 – 389
38. Merchant AA, Matsui W (2010) Targeting Hedgehog — a cancer stem cell pathway. *Clin Cancer Res* 16: 3130 – 3140
39. Liem KF, Ashe A, He M, Satir P, Moran J, Beier D, Wicking C, Anderson KV (2012) The IFT-A complex regulates Shh signaling through cilia structure and membrane protein trafficking. *J Cell Biol* 197: 789 – 800
40. Borowiec AS, Hague F, Harir N, Guenin S, Guerineau F, Gouilleux F, Roudbaraki M, Lassoued K, Ouadid-Ahidouch H (2007) IGF-1 activates hEAG K^+ channels through an Akt-dependent signaling pathway in breast cancer cells: role in cell proliferation. *J Cell Physiol* 212: 690 – 701
41. Darzynkiewicz Z, Juan G, Srour EF (2004) Differential staining of DNA and RNA. *Curr Protoc Cytom* Chapter 7: Unit 7 3
42. Kim S, Zaghloul NA, Bubenshchikova E, Oh EC, Rankin S, Katsanis N, Obara T, Tsiokas L (2011) Nde1-mediated inhibition of ciliogenesis affects cell cycle re-entry. *Nat Cell Biol* 13: 351 – 360
43. Kim J, Jo H, Hong H, Kim MH, Kim JM, Lee JK, Do Heo W, Kim J (2015) Actin remodelling factors control ciliogenesis by regulating YAP/TAZ activity and vesicle trafficking. *Nat Comm* 6: 13
44. Chen Y, Sánchez A, Rubio ME, Kohl T, Pardo LA, Stühmer W (2011) Functional Kv10.1 channels localize to the inner nuclear membrane. *PLoS ONE* 6: e19257
45. Clement CA, Ajbro KD, Koefoed K, Vestergaard ML, Veland IR, de Jesus M, Pedersen LB, Benmerah A, Andersen CY, Larsen LA *et al* (2013) TGF-beta signaling is associated with endocytosis at the pocket region of the primary cilium. *Cell Rep* 3: 1806 – 1814
46. Gómez-Varela D, Zwick-Wallasch E, Knötgen H, Sánchez A, Hettmann T, Ossipov D, Weseloh R, Contreras-Jurado C, Rothe M, Stühmer W *et al* (2007) Monoclonal antibody blockade of the human Eag1 potassium channel function exerts antitumor activity. *Cancer Res* 67: 7343 – 7349
47. Dishinger JF, Kee HL, Jenkins PM, Fan S, Hurd TW, Hammond JW, Truong YN, Margolis B, Martens JR, Verhey KJ (2010) Ciliary entry of the kinesin-2 motor KIF17 is regulated by importin-beta2 and RanGTP. *Nat Cell Biol* 12: 703 – 710
48. Kosugi S, Hasebe M, Tomita M, Yanagawa H (2009) Systematic identification of cell cycle-dependent yeast nucleocytoplasmic shuttling proteins by prediction of composite motifs. *Proc Natl Acad Sci USA* 106: 10171 – 10176
49. MacGrath SM, Koleske AJ (2012) Cortactin in cell migration and cancer at a glance. *J Cell Sci* 125: 1621 – 1626
50. Bershteyn M, Atwood SX, Woo WM, Li M, Oro AE (2010) MIM and cortactin antagonism regulates ciliogenesis and hedgehog signaling. *Dev Cell* 19: 270 – 283
51. Paridaen Judith TML, Wilsch-Bräuninger M, Huttner Wieland B (2013) Asymmetric inheritance of centrosome-associated primary cilium membrane directs ciliogenesis after cell division. *Cell* 155: 333 – 344
52. Gómez-Varela D, Kohl T, Schmidt M, Rubio ME, Kawabe H, Nehring RB, Schäfer S, Stühmer W, Pardo LA (2010) Characterization of Eag1 channel lateral mobility in rat hippocampal cultures by single-particle-tracking with quantum dots. *PLoS ONE* 5: e8858
53. Kohl T, Lörinczi E, Pardo LA, Stühmer W (2011) Rapid internalization of the oncogenic K+channel Kv10.1. *PLoS ONE* 6: e26329
54. Jimenez-Garduno AM, Mitkovski M, Alexopoulos IK, Sanchez A, Stuhmer W, Pardo LA, Ortega A (2014) KV10.1K(+)-channel plasma membrane discrete domain partitioning and its functional correlation in neurons. *Biochim Biophys Acta* 1838: 921 – 931
55. Tucker RW, Scher CD, Stiles CD (1979) Centriole deciliation associated with the early response of 3T3 cells to growth factors but not to SV40. *Cell* 18: 1065 – 1072
56. Zhou Y, Wong C-O, Cho K-J, van der Hoeven D, Liang H, Thakur DP, Luo J, Babic M, Zinsmaier KE, Zhu MX *et al* (2015) Membrane potential modulates plasma membrane phospholipid dynamics and K-Ras signaling. *Science* 349: 873 – 876
57. Jensen VL, Li C, Bowie RV, Clarke L, Mohan S, Blacque OE, Leroux MR (2015) Formation of the transition zone by Mks5/Rpgrip1L establishes a ciliary zone of exclusion (CIZE) that compartmentalises ciliary signalling proteins and controls PIP2 ciliary abundance. *EMBO J* 34: 2537 – 2556
58. Slaats GG, Wheway G, Foletto V, Szymanska K, van Balkom BWM, Logister I, Den Ouden K, Keijzer-Veen MG, Lilien MR, Knoers NV *et al* (2015) Screen-based identification and validation of four novel ion channels as regulators of renal ciliogenesis. *J Cell Sci* 128: 4550 – 4559
59. Wang W, Chen L, Ding Y, Jin J, Liao K (2008) Centrosome separation driven by actin-microfilaments during mitosis is mediated by centrosome-associated tyrosine-phosphorylated cortactin. *J Cell Sci* 121: 1334 – 1343
60. Lee KH, Johmura Y, Yu LR, Park JE, Gao Y, Bang JK, Zhou M, Veenstra TD, Yeon Kim B, Lee KS (2012) Identification of a novel Wnt5a–CK1ε–Dvl2–Plk1-mediated primary cilia disassembly pathway. *EMBO J* 31: 3104 – 3117
61. Nielsen BS, Malinda RR, Schmid FM, Pedersen SF, Christensen ST, Pedersen LB (2015) PDGFRβ and oncogenic mutant PDGFRα D842V promote disassembly of primary cilia through a PLCγ- and AURKA-dependent mechanism. *J Cell Sci* 128: 3543 – 3549
62. Kim M, Kim M, Lee M-S, Kim C-H, Lim D-S (2014) The MST1/2-SAV1 complex of the Hippo pathway promotes ciliogenesis. *Nat Commun* 5: 5370
63. Troilo A, Alexander I, Muehl S, Jaramillo D, Knobeloch KP, Krek W (2014) HIF1alpha deubiquitination by USP8 is essential for ciliogenesis in normoxia. *EMBO Rep* 15: 77 – 85

64. Delling M, DeCaen PG, Doerner JF, Febvay S, Clapham DE (2013) Primary cilia are specialized calcium signalling organelles. *Nature* 504: 311 – 314
65. Vadhvani M, Schwedhelm-Domeyer N, Mukherjee C, Stegmüller J (2013) The CENTROSOMAL E3 ubiquitin ligase FBXO31-SCF regulates neuronal morphogenesis and migration. *PLoS ONE* 8: e57530
66. Schindelin J, Arganda-Carreras I, Frise E, Kaynig V, Longair M, Pietzsch T, Preibisch S, Rueden C, Saalfeld S, Schmid B *et al* (2012) Fiji: an open-source platform for biological-image analysis. *Nat Methods* 9: 676 – 682